International Journal of GEOMATE, July, 2017, Vol. 13, Issue 35, pp. 8 -15
Geotec., Const. Mat. & Env., ISSN:2186-2990, Japan, DOI: http://dx.doi.org/10.21660/2017.35.6623

STRENGTH AND DEFORMATION CHARACTERISTICS OF EPS BEAD-MIXED SAND

Agawit Thaothip [1] and *Warat Kongkitkul [2]

[1,2]Department of Civil Engineering, Faculty of Engineering, King Mongkut's University of Technology Thonburi, Thailand

*Corresponding Author, Received: 27 June 2016, Revised: 15 July 2016, Accepted: 26 Nov. 2016

ABSTRACT: In this research, a study on strength and deformation characteristics of expanded polystyrene (EPS) bead-mixed sand was comprehensively conducted. A series of standard Proctor compaction tests were conducted to determine the proper amount water for use in the mixing between EPS bead and sand at the volumetric ratio of 1:1. A special series of drained triaxial compression tests were performed on the sand-EPS bead mixture (SEM) specimens. Various loading histories, consisting of: i) monotonic loading (ML) at different constant strain rates; ii) sustained (creep) loading (SL); iii) cyclic loading with small strain-amplitude (CL); and iv) stepwise changes in the strain rate during otherwise ML, were employed in this study. These loading histories were used to evaluate the elastic and viscous properties of the SEM. Then these properties were also compared with the ones obtained from the sand alone under similar loading conditions. It is found that the elastic and viscous properties of the SEM are qualitatively similar to those of sand alone. They are different in terms of quantity. A non-linear three-component (NTC) model was used to simulate the elasto-viscoplastic deformations of the SEM. The simulations are well successful by using the model parameters determined especially for the SEM sand under the conventional model framework.

Keywords: Creep, Elastic, EPS bead, EPS bead-mixed sand, Non-linear three-component model, Strain rate, Triaxial compression test.

1. INTRODUCTION

Settlement of road embankment constructed on the soft clay deposit by its primary consolidation is a crucial problem. This is especially the case with the bridge approach where differential settlement can result, and thus leads to danger for the drivers. At present, there are many mitigation techniques proposed which can be categorised into two groups; i.e., i) improvement of the soft clay layer by mixing with cement or other relevant additives [1]-[4]; and ii) reducing the surcharge on the soft clay layer by using the lightweight fill materials [5], [6]. This research interests on the strength and deformation properties of the latter group. A sand-expanded polystyrene (EPS) bead mixture (SEM) [7] was prepared by mixing at the ratio of 1:1 by volume, and therefore, the unit weight of SEM became about a half of that of the sand alone. When used as a refilling material to replace the original sand fill, the unit weight of SEM is sufficient low so as to prevent the primary consolidation of the soft clay to further develop, if the degree of consolidation of more than a certain level had been achieved.

In view of the above, a series of special air-drained triaxial compression tests [8] were performed in this study. Various loading histories including: i) continuous monotonic loading with different constant strain rates; ii) sustained (creep) loading; iii) cyclic loading; and iv) stepwise changes in the applied shearing strain rate, were used to evaluate strength properties, and elastic and viscous properties of SEM. Test results of SEM are presented and compared with those of the sand alone. Lastly, an elasto-viscoplastic non-linear three-component (NTC) model was used for simulations of test results of SEM observed in the present study.

2. TEST MATERIALS

There are two test materials used in the present study. They are sand and EPS bead.

2.1 Sand

A cleaned riverbed sand was used. To control its gradation, the portion that passes through sieve No. 40 but retains on sieve No. 50 was mixed with the other portion that passes through sieve No. 50 but retains on sieve No. 100 at the ratio of 1:1 by mass. The gradation curve thus obtained is shown in Fig. 1.

2.2 EPS Beads

A type of EPS bead was used. Its diameter is around 1-2 mm. The absolute density is 32.9 kg/m^3.

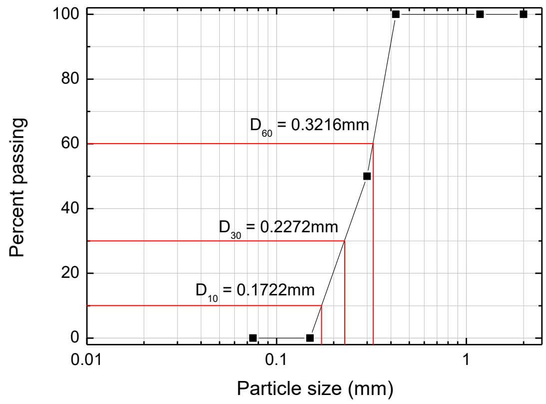

Fig. 1 Particle size distribution of sand.

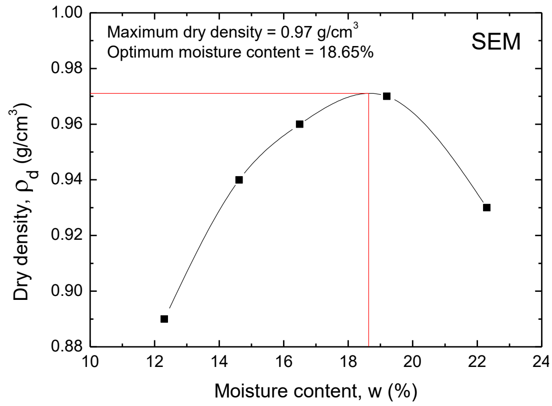

Fig. 2 Compaction curve by standard Proctor compaction test on SEM.

3. TEST METHODS

3.1 Standard Proctor Compaction Test

The purpose of this test is to determine the maximum dry density and the optimum moisture content of SEM. Fig. 2 shows the compaction curve which defines the optimum moisture content (OMC) of 18.65% and the maximum dry density of 0.97 g/cm^3.

3.2 Air-Drained Triaxial Compression Tests

The purpose of this test is to evaluate the strength and deformation properties of SEM. The specimen is cylindrical in the shape. It is 150 mm high by 70 mm in diameter. Triaxial specimens were prepared by tamping the SEM layered in the mould such that the density meets the target value (0.97 g/cm^3).

Table 1 Triaxial compression test program

Test	S	E	W	SP	σ_3	$\dot{\varepsilon}_v$
SND01	875	-	163	ML	25	0.15
SND02	875	-	163	ML	50	0.15
SND03	875	-	163	ML	75	0.15
SND04	875	-	163	ML	100	0.15
SEM01	550	12	105	ML	25	0.15
SEM02	550	12	105	ML	50	0.15
SEM03	550	12	105	ML	75	0.15
SEM04	550	12	105	ML	100	0.15
SEM05	550	12	105	ML	100	0.05
SEM06	550	12	105	SL,CL	100	0.05
SEM07	550	12	105	SL,CL	100	0.05
SEM08	550	12	105	ML	100	0.50
SEM09	550	12	105	SL,CL	100	0.50
SEM10	550	12	105	SL,CL	100	0.50
SEM11	550	12	105	SS	100	0.05
SEM12	550	12	105	SS	100	0.05

Note: S = sand (g); E = EPS bead (g); W = water (g); SP = shearing patterns; σ_3 = confining pressure (kPa); $\dot{\varepsilon}_v$ = basic vertical strain rate (%/min) during ML; SND = tests on sand alone; and SEM = tests on sand-EPS bead mixture

Four loading patterns were employed. They are: i) continuous monotonic loading with constant strain rate (ML); ii) sustained loading (SL); iii) cyclic loading (CL); and iv) stepwise changes in the applied shearing strain rate (SS). Triaxial compression test program is shown in Table 1.

4. TEST RESULTS AND DISCUSSIONS

4.1 Monotonic Loading Test Results

From ML tests, deviator stress (q)-axial strain (ε_a) relationships can be compared between the sand alone (Fig. 3(a)) and the SEM (Fig. 3(b)) can be compared. It can be observed from Figs. 3(a) and 3(b) that the q-ε_a relations exhibit a strain-hardening behaviour until achieving the respective peaks, and then show a strain-softening behaviour toward the respective residual states. The behaviours described above are qualitatively similar between the sand alone and the SEM specimens. This may imply that the sand in the SEM matrix plays a major role to control the global behaviours of the SEM.

Shear strength parameters at the peak and the residual states of the sand alone and the SEM are listed in Table 2. The peak and residual friction angles of the sand alone are noticeably greater than the corresponding values of the SEM. On the other hand, cohesion at the peak state of the sand alone is smaller than that of the SEM.

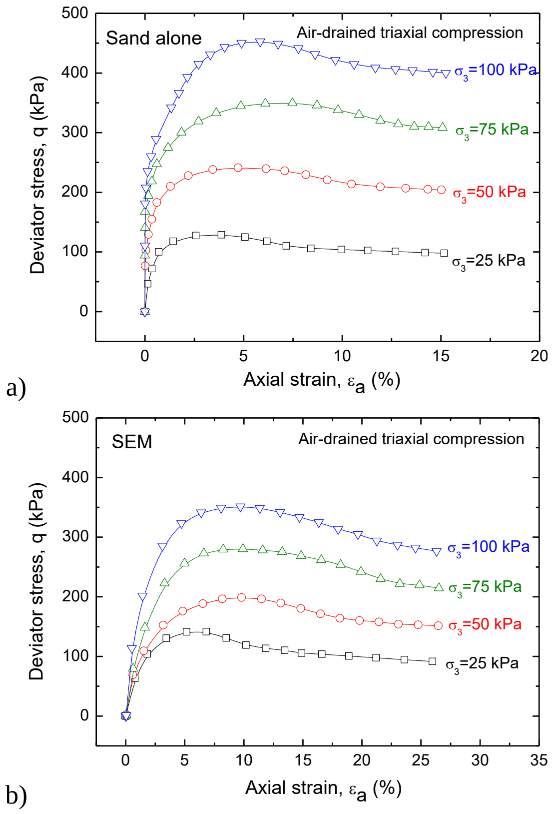

Fig. 3 Deviator stress (q)-axial strain (ε_a) relations from continuous ML triaxial compression tests on: (a) sand alone; and (b) SEM

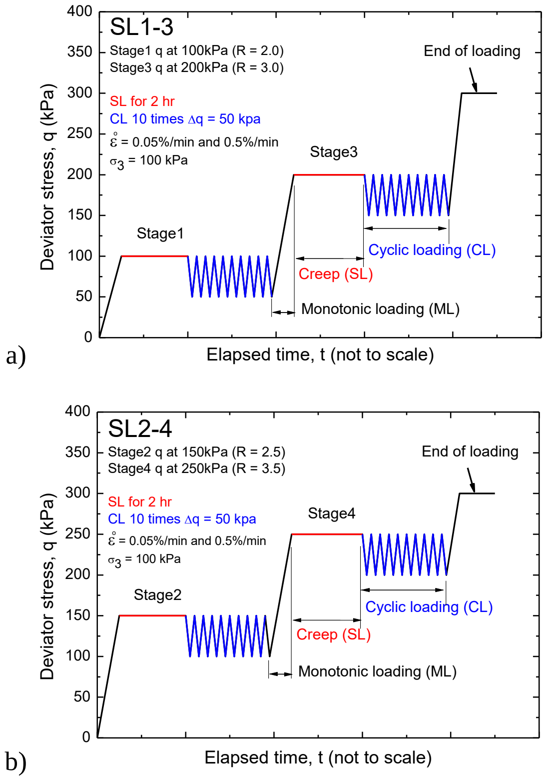

Fig. 4 Loading histories used to evaluate elastic modulus and creep behaviours of SEM at: (a) R =2.0 & 3.0 (SL1-3); and (b) R =2.5 & 3.5 (SL2-4).

Table 2 Shear strength parameters of sand alone and SEM

Sample	State	Cohesion (kPa)	Friction angle (°)
Sand alone	Peak	5.0	43.1
	Residual	0.0	42.0
SEM	Peak	16.5	36.0
	Residual	0.0	34.5

4.2 Elastic Modulus from CL Tests

Two patterns of loading histories, used to evaluate the elastic modulus and the creep behaviours of SEM, are shown in Figs. 4(a) and 4(b). In these tests, ML was firstly applied until the specified deviator stress of 100, 150, 200 or 250 kPa was achieved and then sustained loading (SL) which lasted for two hours was applied. Next cyclic loadings (CL) with a double stress-amplitude of 50 kPa were applied for 10 cycles. Two values of strain rate equal to 0.05 and 0.5 %/min were employed during ML and CL in their courses (Figs. 4(a) and 4(b)). Test results thus obtained are shown in Figs. 5(a) and 5(b) for the strain rate of 0.05 and 0.5 %/min, respectively. It can be clearly observed that, upon the restart of ML after the last CL at the highest deviator stress level in a CL course, the q-ε_a relation tends to rejoin to the relation that was obtained from the respective continuous ML test, and importantly, the peak deviator stress is maintained. Thus it can be postulated that, although creep strain of SEM is obvious, it does not degrade the SEM's shear strength.

Unloading braches of CL of the last five loops were exaggerated as shown in Fig. 6. To determine the values of quasi-elastic Young's modulus (E_{eq}) [9], lines were best-fitted to these respective unloading branches. Then the slopes of there lines were averaged and accounted as the representative of E_{eq} for the deviator stress level at which it was determined. Next the E_{eq} value was converted to be represented in terms of R, where R is the stress ratio equal to σ_1/σ_3. Fig. 7 shows the relation between E_{eq} (expressed in terms of R) and R, plotted in the full-log scale. It can be seen that E_{eq} is not constant but increases with an increase in the stress ratio. For the same stress ratio, the E_{eq} of the sand alone is noticeably greater than that of the SEM. The dependency of elastic modulus with the stress level observed with the sand alone and the SEM is qualitatively similar and can be expressed with hypo-elasticity expressed by Eq. 1.

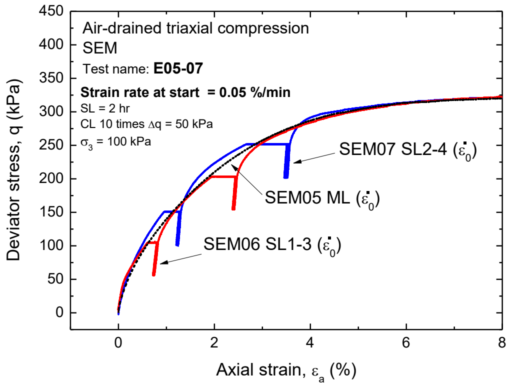

a)

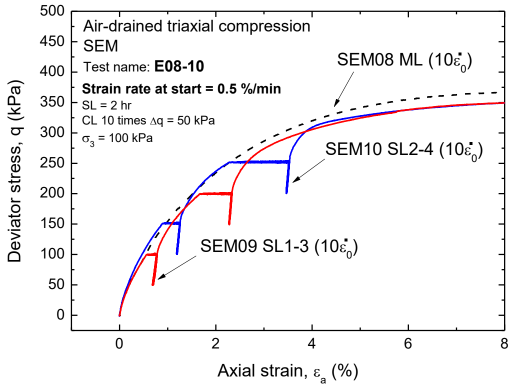

b)

Fig. 5 Deviator stress-axial strain relations of SEM obtained from tests with the intermissions of SL and CL; the strain rate during ML and CL is: (a) 0.05 %/min; and (b) 0.5 %/min

$$E_{eq} = E_0 \left(R\right)^m \tag{1}$$

where $E_0\left(R/\%\right)$ = 7.20 and 5.66 for the sand alone and the SEM, respectively; m = 0.576 and 0.485 for the sand alone and the SEM, respectively.

4.3 Creep Loading Test Results

Fig. 8 compares creep axial strain of SEM developed for two hours between the sustained loadings with the initial strain rates of 0.05 %/min and 0.5 %/min. The test results reveal that creep axial strain increases with time. However, the creep strain rate decreases with time towards nearly zero at the end of creep. Creep strain developed by sustained loading for two hours increases with the stress ratio, and at the same time, creep of SEM obtained with the initial strain rate of 0.5 %/min is significantly larger than the one with the initial strain rate of 0.05 %/min. This shows the influence of strain rate at the start of creep on the development of creep strain with time. In order to compare the creep axial strains having different initial strain rates, they were corrected to a common initial strain rate of 3.5 x 10^{-4} %/min. Then the comparison of creep axial strains between the sand alone and the SEM under the same initial strain rate condition is shown in Fig. 9. The two different relations for

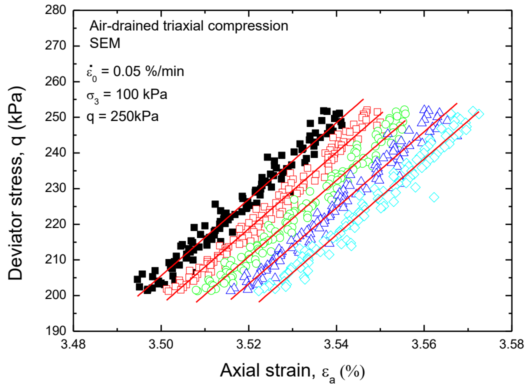

Fig. 6 Unloading branches of the last five loops of a CL course with the respective best-fitted lines to determine the quasi-elastic modulus

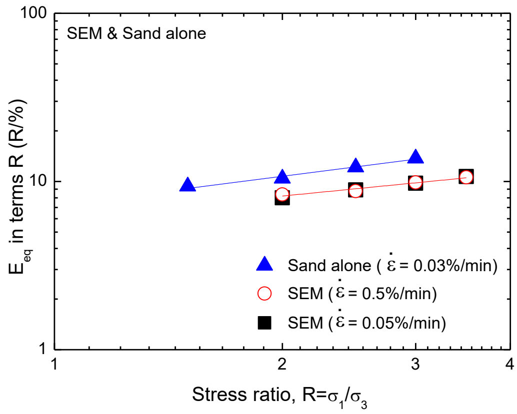

Fig. 7 Comparison of $E_{eq} - R$ relations between sand alone and SEM

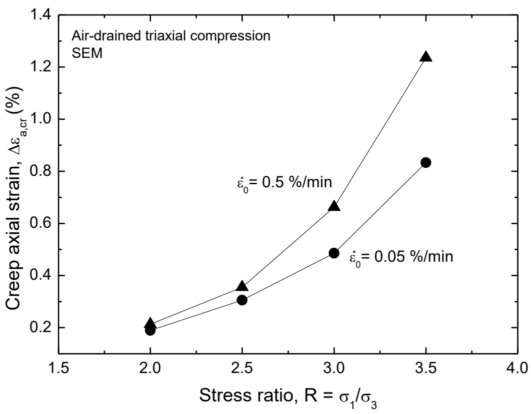

Fig. 8 Comparison of creep axial strains of SEM for two hours between the initial strain rates of 0.05 %/min and 0.5 %/min

SEM shown in Fig. 8 are now becoming very close to each other in Fig. 9. The trend of increasing of creep axial strain with the increasing stress ratio is obvious for both sand alone and SEM. However, creep of SEM is noticeably greater than the one of the sand alone as shown in Fig. 9.

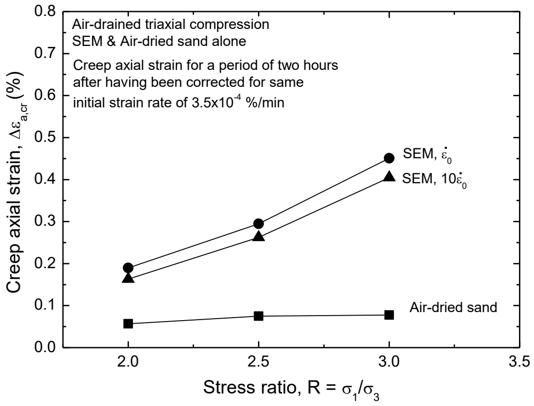

Fig. 9 Comparisons of creep axial strains after having been corrected for the same initial strain rate of 3.5 x 10^{-4} %/min between sand alone and SEM

4.4 Strain Rate Responses of SEM

Responses of SEM to changes in the strain rate were also studied in this research. To quantify the viscous responses, stepwise changes in the applied shearing strain rate were performed. In these tests, the basic reference strain rate ($\dot{\varepsilon}_0$) of 0.05%/min was firstly selected. Different strain rates that are slower and faster than $\dot{\varepsilon}_0$ for 10 and 100 times and also the $\dot{\varepsilon}_0$ were then specified into a set. During a test, the shearing strain rate was stepwise changed many times from a value to the other value specified in the set. Fig. 10 shows relationship between the stress ratio and the irreversible axial strain obtained with the above-mentioned changings in the strain rate. It can be readily seen that upon stepwise changes in the strain rate, the stress-strain relation exhibited stress jumps. These stress jumps are responses due to the viscosity of SEM. To quantify the viscosity of SEM, jump in the stress ratio upon a stepwise increase or decrease in the strain rate was defined as shown in Fig. 11. Then the measured stress ratio jumps were normalised with the stress ratio immediately before the jump (ΔR/R), and then plotted against the ratio of strain rate after and before stepwise change, as shown in Fig. 12. The slope of the line best-fitted to the data points shown in Fig. 12 (Eq. (2)) is called the rate-sensitivity coefficient (β) [10], [11].

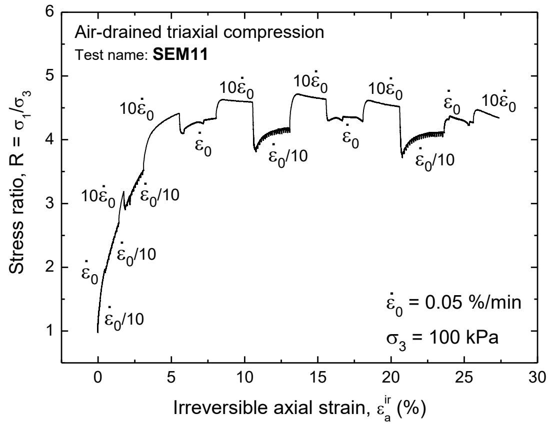

Fig. 10 Relationship between stress ratio and irreversible axial strain of SEM obtained from a test with multiple changes in the strain rate

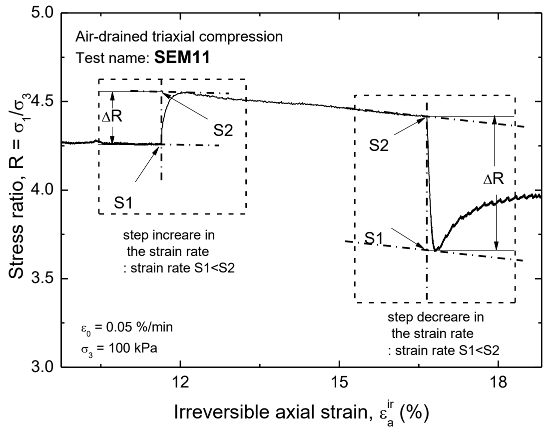

Fig. 11 Definitions of stress jumps upon a step increase and a step decrease in the irreversible strain rate

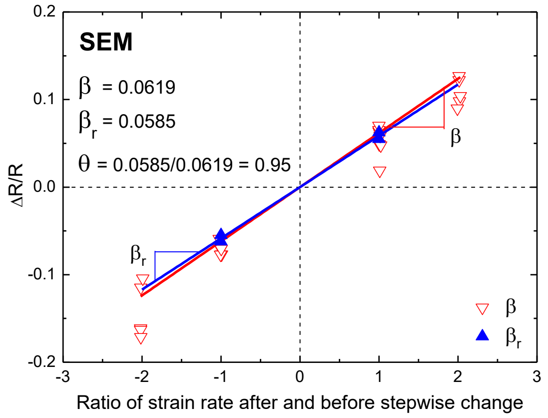

Fig. 12 Determination of rate-sensitivity coefficient from relationship between the normalised stress ratio jump and the ratio of strain rate after and before stepwise change

$$\frac{\Delta R}{R} = \beta \log_{10}\left(\frac{\dot{\varepsilon}^{ir}_{after}}{\dot{\varepsilon}^{ir}_{before}}\right) \tag{2}$$

The β value of SEM determined from this study is 0.0619. On the other hand, from previous studies on other standard sands by performing stepwise changings in the strain rate during triaxial tests [12], [13], the β values are equal to 0.0226, 0.0195, and 0.0195 for Toyoura sand, Albany sand, and Monterey sand, respectively. Therefore, SEM is more sensitive to changes in the strain rate than typical sands for about three times, which may be due to the inclusion of EPS bead into the matrix.

5. SIMULATIONS

5.1 Non-Linear Three-Component Model

A non-linear three-component (NTC) model (Fig. 13) was used to simulate rate-dependent characteristics (e.g., creep, jump in the stress ratio) of SEM. The three components are elastic, inviscid, and viscous components. Total stress ratio (R) consists of the inviscid and the viscous components (R^f and R^v) while strain rate ($\dot{\varepsilon}$) the elastic ($\dot{\varepsilon}^e$) and the irreversible ($\dot{\varepsilon}^{ir}$) components.

Elastic modulus (E_{eq}) of the elastic component, which is dependent of stress ratio level (Fig. 7), is determined by a hypo-elasticity model (Eq. 1). The elastic strain rate can then be calculated from Eq. 3 [14], [15].

$$\dot{\varepsilon}^e = R/E_{eq} \tag{3}$$

Inviscid stress ratio (R^f)-irreversible axial strain (ε_a^{ir}) relation of the inviscid component, which is independent of any strain rate effect and called the reference curve, is determined from the functional form shown in Eq. 4.

$$R^f = P_1 + \left(P_2 + P_3\varepsilon_a^{ir}\right)\left\{1 - \exp\left[-P_4\left(\varepsilon_a^{ir}\right)^{P_5} - P_6\frac{\varepsilon_a^{ir}}{P_2}\right]\right\} \tag{4}$$

where $P_1 - P_5$ are constants that are determined from the regression analysis such that Eq. 4 is best-fitted to the respective measured R- ε_a^{ir} relation that is extrapolated to zero-strain rate.

The rate-dependent responses of SEM can be observed not only with creep by sustained loading (Fig. 5) and stress ratio jumps by changes in the strain rate (Fig. 10) but also with R-ε_a relations by continuous ML tests with different strain rates as shown in Fig. 14. At the same ε_a, it is obvious that R for the faster strain rate is greater than the value for the slower strain rate. This difference in the R value along continuous ML R-ε_a relations with different strain rates is referred as residual state of rate-dependency [12]. In Fig. 14, imaginary stress

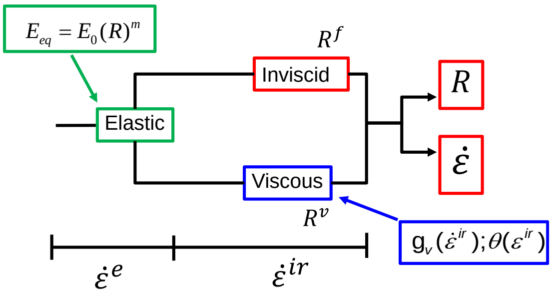

Fig. 13 Non-linear three-component model [10]-[12]

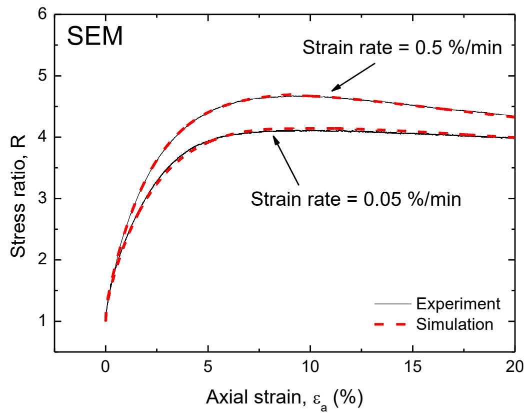

Fig. 14 Simulations of continuous ML tests on SEM with different but constant strain rates of 0.05 and 0.5 %/min

ratio jumps were imposed between the two R-ε_a relations, and then coefficient of rate-sensitivity at the residual state (β_r) is then determined as shown in Fig. 12. Then the viscosity type parameter (θ) [12] can then be determined from Eq. 5.

$$\theta = \beta_r/\beta \tag{5}$$

It was also found with SEM that, similar to many other geomaterials [12], the θ value is not constant but dependent on the irreversible strain, and can be expressed with Eq. 6.

$$\theta(\varepsilon^{ir}) = \frac{\theta_{ini} + \theta_{end}}{2} + \frac{\theta_{ini} - \theta_{end}}{2}\cos\left[\pi\left(\frac{\varepsilon^{ir}}{\varepsilon^{ir}_{\theta}}\right)^{c}\right];\ \varepsilon^{ir} < \varepsilon^{ir}_{\theta} \tag{6a}$$

$$\theta(\varepsilon^{ir}) = \theta_{end};\ \varepsilon^{ir} \geq \varepsilon^{ir}_{\theta} \tag{6b}$$

where θ_{ini} and θ_{end} are the initial and residual values of transition of the θ value; c and $\varepsilon^{ir}_{\theta}$ are constants. The viscous stress ratio (R^v) can be determined from Eq. 7 [12].

$$R^{v}(\varepsilon^{ir},\dot{\varepsilon}^{ir},h_s)=\theta(\varepsilon^{ir})\cdot R^{v}_{iso}(\varepsilon^{ir},\dot{\varepsilon}^{ir})+\{1-\theta(\varepsilon^{ir})\}\cdot R^{v}_{G.TESRA}(\varepsilon^{ir},\dot{\varepsilon}^{ir},h_s) \quad (7a)$$

$$R^{v}_{iso}(\varepsilon^{ir},\dot{\varepsilon}^{ir})=R^{f}(\varepsilon^{ir})\cdot g_v(\dot{\varepsilon}^{ir}) \quad (7b)$$

$$R^{v}_{G.TESRA}(\varepsilon^{ir},\dot{\varepsilon}^{ir},h_s)=\int_{\tau=\varepsilon_1^{ir}}^{\varepsilon^{ir}}\left[dR^{v}_{iso}\right]_{(\tau)}\cdot[r_1(\varepsilon^{ir})]^{\varepsilon^{ir}-\tau} \quad (7c)$$

$$g_v(\dot{\varepsilon}^{ir})=\alpha\cdot[1-\exp\{1-(\frac{\left|\dot{\varepsilon}^{ir}\right|}{\dot{\varepsilon}^{ir}_{r}}+1)^{m}\}] \quad (7d)$$

where α, m, $\dot{\varepsilon}^{ir}_{r}$ are constants, while r_1 is a decay parameter varying with the irreversible strain in a manner similar to that of the viscosity type parameter (Eq. 6).

5.2 Simulation Results

Fig. 14 compares the R-ε_a relations between the experimental and simulation results from continuous ML on SEM with the strain rates equal to 0.05 and 0.5 %/min. It can be readily seen that the NTC model can well-successfully simulate all the R-ε_a characteristics that are different by the strain rate effects.

Fig. 15(a) compares R-ε_a relations of SEM subjected to SL during otherwise ML at the strain rate of 0.5 %/min between the experimental and simulation results. It can be seen that not only the development of axial strain under a constant stress ratio condition (creep) but also the behaviour in that the R-ε_a relation rejoins to the one that would be obtained from continuous ML can successfully be simulated. Fig. 15(b) compares the creep axial strains for different stress ratio values. The behaviours in that the creep axial strain increases with an increase in the stress ratio and also with an increase in the initial strain rate at the start of creep can be well-simulated. Thus the NTC model can be used to predict the time-dependent (rate-dependent) creep deformation of SEM.

Fig. 16 compares R-ε_a relations of SEM subjected to stepwise changes in the strain rate between the experimental and simulation results. All the sudden increases and decreases of stress ratio by respectively stepwise increases and decreases in the strain rate can be well-simulated. The NTC model therefore has a great potential to predict the rate-dependent deformation characteristics of SEM evaluated by the experiments in the present study.

6. CONCLUSIONS

The following conclusions can be derived from the air-drained triaxial compression test results and their simulations.

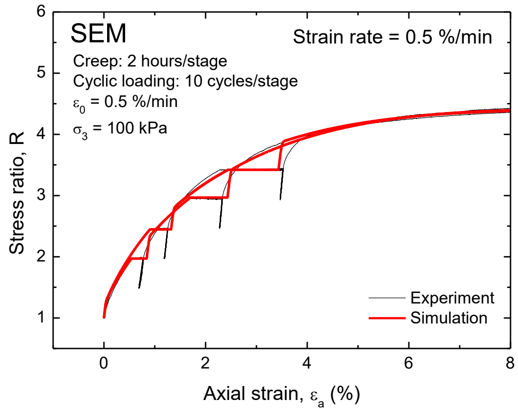

a)

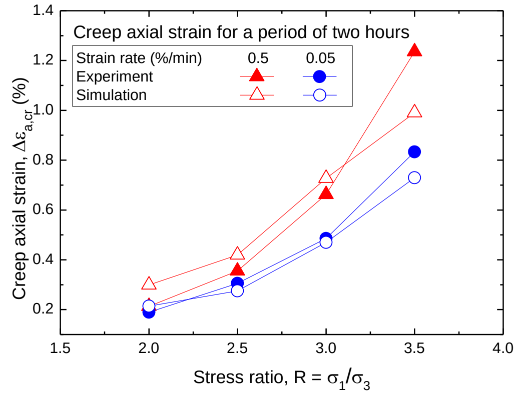

b)

Fig. 15 Simulations of 2-hr SL tests on SEM during otherwise ML: a) comparisons of R-ε_a relation with the strain rate during ML of 0.5 %/min; and b) comparisons of creep axial strain for different stress ratios

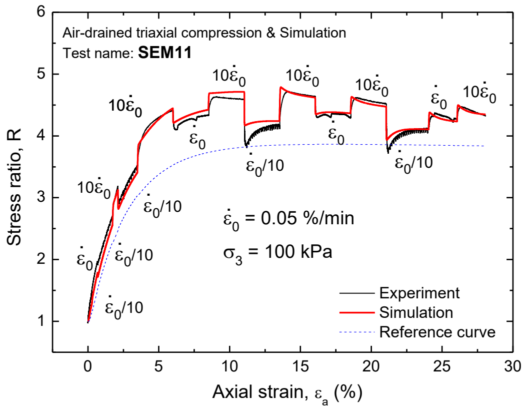

Fig. 16 Simulations of stepwise changes in the strain rate applied to SEM

1. Peak and residual friction angles of SEM are noticeably smaller than those of sand alone.
2. Elastic Young's moduli of air-dried sand alone and SEM are not constant but increase with an increase in the axial stress. At the same axial stress, the elastic Young's modulus of SEM is quite smaller than that of air-dried sand alone.

3. SEM exhibited creep strain significantly upon the applied sustained loading. The creep strain increases with an increase in the shear stress level and also increases with an increase in the strain rate at the start of creep. Creep strain of SEM is significantly larger than the one of sand alone. Yet, by ML at the end of creep, the stress-strain relation of SEM rejoins to the one that is obtained by continuous ML with the same strain rate, and thus, the peak shear strength is maintained. Therefore, creep of SEM is not a degradation phenomenon.
4. SEM is more sensitive to the strain rate than the air-dried sand alone. This also results in a greater amount of creep developed under otherwise the same conditions.
5. NTC model can successfully simulate the stress-strain-time behaviours of SEM, taken into account the dependency of elastic Young's modulus with the axial stress and the evaluated and quantified viscous properties. Moreover, this model can successfully predict the creep strain developed during sustained loading.

7. ACKNOWLEDGEMENTS

The authors would like to acknowledge the support from Department of Civil Engineering, King Mongkut's University of Technology Thonburi (CE-KMUTT-FTERO 6001). Thanks are also extended to Thailand Research Fund (TRF), Thailand. The EPS bead used in this study was provided from Polyfoam Industries Co., Ltd.

8. REFERENCES

[1] Chida S, "Dry jet mixing method-State of the Art on Improvement Methods for Soft Ground", J. of Japan Society of Soil Mechanics and Foundation Engineering, Vol.185, No.2, 1982, pp.69-76.

[2] Kawasaki T, Niina A, Saitoh S, Suzuki Y, and Honjo Y, "Deep mixing method using cement hardening agent", Proceedings of 10th International Conference on Soil Mechanics and Foundation Engineering, Stockholm, 1981, pp.721-724.

[3] Miura N, Koga Y, and Nishida K, "Application of a deep mixing method with quicklime for Ariake-clay ground", J. of Japanese Society of Soil Mechanics and Foundation Engineering, Vol.34, No.4, 1986, pp.5-11.

[4] Terashi M, Tanaka H, and Okumura T. "Engineering properties of lime treated marine soils and deep mixing method", Proceedings of 6th Asian Regional Conference on Soil Mechanics and Foundation Engineering, Vol.1, 1979, pp.191-194.

[5] Horvath JS, "The compressible inclusion function of EPS geofoam", Geotextiles and Geomembranes, Vol.15, Nos.1-3, February-June, 1997, pp. 77-120.

[6] Stark TD, Arellano D, Horvath JS, and Leshchinsky D, Guideline and Recommended Standard for Geofoam Applications in Highway Embankments, NCHRP Report 529, Transportation Research Board, 2004.

[7] Edincliler A and Ozer AT, "Effects of EPS bead inclusions on stress–strain behaviour of sand". Geosynthetics International, Vol.21, No.2, 2014, pp.89-102.

[8] Das BM, Fundamentals of Geotechnical Engineering, 4th Edition, Cengage Learning, Canada, 2013.

[9] Kongkitkul W, Tabsombut W, Jaturapitakkul C, and Tatsuoka F, "Effects of temperature on the rupture strength and elastic stiffness of geogrids", Geosynthetics International, Vol.19, No.2, April, 2012, pp.106-123.

[10] Tatsuoka F, Ishihara M, Di Benedetto H, and Kuwano R, "Time-dependent shear deformation characteristics of geomaterials and their simulation", Soils and Foundations, Vol.42, No.2, 2002, pp.103-129.

[11] Di Benedetto H, Tatsuoka F, and Ishihara M, "Time-dependent shear deformation characteristics of sand and their constitutive modelling", Soils and Foundations, Vol. 42, No.2, 2002, pp.1-22.

[12] Tatsuoka F, Di Benedetto H, Enomoto T, Kawabe S, and Kongkitkul W, "Various viscosity types of geomaterials in shear and their mathematical expression", Soils and Foundations, Vol.48, No.1, February, 2008, pp. 41-60.

[13] Kiyota T and Tatsuoka F, "Viscous property of loose sand in triaxial compression, extension and cyclic loading", Soils and Foundations, Vol. 46, No.5, 2006, pp.665-684.

[14] Hoque E and Tatsuoka F, "Anisotropy in elastic deformation of granular materials", Soils and Foundations, Vol.38, No.1, 1998, pp.163-179.

[15] Kongkitkul W, Musika N, Tongnuapad C, Jongpradist P, and Youwai S, "Anisotropy in compressive strength and elastic stiffness of normal and polymer-modified asphalts", Soils and Foundations, Vol. 54, No. 2, April, 2014, pp. 94-108.